

See discussions, stats, and author profiles for this publication at: <https://www.researchgate.net/publication/263468768>

# Influence of Shell Thickness and Surface Passivation on PbS/CdS Core/Shell Colloidal Quantum Dot Solar Cells

ARTICLE in CHEMISTRY OF MATERIALS · JUNE 2014

Impact Factor: 8.35 · DOI: 10.1021/cm501595u

---

CITATIONS

20

READS

212

## 10 AUTHORS, INCLUDING:



Cheng Cheng

University of Oxford

7 PUBLICATIONS 215 CITATIONS

[SEE PROFILE](#)



Samuel D Stranks

Massachusetts Institute of Technology

58 PUBLICATIONS 2,667 CITATIONS

[SEE PROFILE](#)



Judy S. Kim

University of Oxford

36 PUBLICATIONS 429 CITATIONS

[SEE PROFILE](#)



Angus I Kirkland

University of Oxford

259 PUBLICATIONS 3,712 CITATIONS

[SEE PROFILE](#)

# Influence of Shell Thickness and Surface Passivation on PbS/CdS Core/Shell Colloidal Quantum Dot Solar Cells

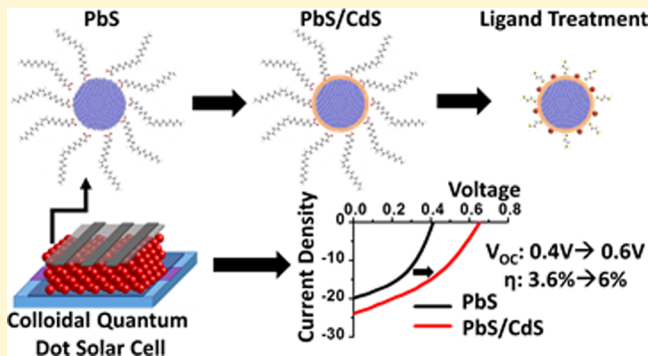
Darren C. J. Neo,<sup>†,‡</sup> Cheng Cheng,<sup>†</sup> Samuel D. Stranks,<sup>§</sup> Simon M. Fairclough,<sup>†</sup> Judy S. Kim,<sup>†</sup> Angus I. Kirkland,<sup>†</sup> Jason M. Smith,<sup>†</sup> Henry J. Snaith,<sup>§</sup> Hazel E. Assender,<sup>†,‡</sup> and Andrew A. R. Watt\*,<sup>†,‡</sup>

<sup>†</sup>Department of Materials, University of Oxford, 16 Parks Road, Oxford OX1 3PH, United Kingdom

<sup>§</sup>Department of Physics, Clarendon Laboratory, Parks Road, Oxford OX1 3PU, United Kingdom

## Supporting Information

**ABSTRACT:** Cation-exchange has been used to synthesize PbS/CdS core/shell colloidal quantum dots from PbS starting cores. These were then incorporated as the active material in solar cell test devices using a solution-based, air-ambient, layer-by-layer spin coating process. We show that core/shell colloidal quantum dots can replace their unshelled counterparts with a similar band gap as the active layer in a solar cell device, leading to an improvement in open circuit voltage from 0.42 to 0.66 V. This improvement is attributed to a reduction in recombination as a result of the passivating shell. However, this increase comes at the expense of short circuit current by creating a barrier for transport. To overcome this, we first optimize the shell thickness by varying the conditions for cation-exchange to form the thinnest shell layer possible that provides sufficient surface passivation. Next, ligand exchange with a combination of halide and bifunctional organic molecules is used in conjunction with the core/shell strategy. Power conversion efficiencies of  $5.6 \pm 0.4\%$  have been achieved with a simple heterojunction device architecture.



## INTRODUCTION

Colloidal quantum dots (CQDs) are a promising material for use in photovoltaic (PV) technology. They allow low-cost versatile device processing<sup>1–3</sup> and might be used to exploit new ideas in quantum physics<sup>4–8</sup> and materials chemistry<sup>9,10</sup> in a bid to overcome the Shockley-Quessier limit.<sup>11,12</sup> Lead sulfide (PbS) CQDs currently top the photovoltaic efficiency tables<sup>13</sup> in this class, with great developments being made by improving junction architecture,<sup>13</sup> carrier properties,<sup>14–16</sup> and solution deposition chemistry.<sup>17,18</sup> However, efficiencies still lag behind competing technologies, like dye-sensitized solar cells, largely because of comparatively poor electronic properties.

The limiting factor for the current generation of CQD devices are the lower than expected open-circuit voltage ( $V_{OC}$ )<sup>19</sup> values, which are attributed to the high density of defect states.<sup>20</sup> Electronically active CQD thin films are produced by exchanging the long-chain ligands used to synthesize and stabilize the CQD for a shorter linker ligand, which allows electronic coupling between neighboring CQDs in the film. Currently, a postdeposition solid-state treatment is used to produce the best devices.<sup>21–23</sup> However, despite the improvements made, this exchange process has been shown to be imperfect, causing surface defects which increase recombination and nonradiative losses, thus directly reducing  $V_{OC}$ .<sup>21</sup> These defects are caused by incomplete ligand coverage<sup>24</sup> or the inherent instability of the more labile shorter ligands.<sup>25</sup> In addition, postdeposition exchange is highly dependent on

optimizing ligand concentration, solvation, impurity elimination, and processing environment.<sup>17,26,27</sup> Ip et al. recently investigated the role of ligand coverage and demonstrated that a combination of short bifunctional organic and atomic halide ligands results in nearly complete CQD surface passivation. Using transient photovoltage measurements, the authors showed a reduction in defect density as compared to an organic ligand-only treatment.<sup>21</sup> However, this strategy is strongly dependent on the stability of ligands.

In photoluminescent applications of CQD such as biolabeling,<sup>28</sup> the issue of surface passivation is addressed by having a shell of another wider band gap semiconductor (forming a type I heterostructure) grown around the CQD. This shell passivation method has been shown to be stable and effective,<sup>29–32</sup> giving rise to higher photoluminescence quantum yields, longer decay lifetimes and even greater chemical and environmental stability.<sup>29,33,34</sup> While employing a coating of a wider band gap material on a nanocrystal sensitizer is a well-established procedure in quantum dot-sensitized solar cells,<sup>35</sup> reports of using core/shell quantum dots as both the light absorber and the active transport material are scarce. This is possibly because a thick shell layer of a type I heterostructure impedes exciton dissociation, charge extraction,

Received: May 3, 2014

Revised: June 5, 2014



ACS Publications

© XXXX American Chemical Society

A

dx.doi.org/10.1021/cm501595u | Chem. Mater. XXXX, XXX, XXX–XXX

and transport.<sup>36</sup> Zamkov and co-workers showed that having a CdS shell on PbS quantum dot improves passivation and that the distance between PbS quantum dots and hence the thickness of CdS layer impact carrier mobility and device performance.<sup>37,38</sup> Etgar et al. also showed that a type II lead selenide/lead sulfide core/shell quantum dot can improve exciton dissociation.<sup>39</sup> This paper builds upon these studies to increase device efficiencies, and to investigate the effect of shell thickness and surface chemistry on device performance. This is done by developing a passivation strategy that uses the synergistic effect of a core/shell structure and ligands coordination to passivate CQD surfaces.

## EXPERIMENTAL SECTION

**Material.** Lead oxide yellow (PbO, 99.9%) was purchased from Acros Organics. Oleic acid (OA, 90%), 1-octadecene (ODE, 90%), bis(trimethylsilyl) sulfide ((TMS)<sub>2</sub>S, synthesis grade), cadmium acetate hydrate (Cd(Ac)<sub>2</sub>, 99.99%), poly(3,4-ethylenedioxythiophene)-poly(styrenesulfonate) (PEDOT:PSS, 1.3 wt % in water, conductive grade), 1,2-ethanedithiol (EDT, >98%), cetyltrimethylammonium bromide (CTAB, >98%), and anhydrous cadmium chloride (CdCl<sub>2</sub>, 99%) were purchased from Sigma-Aldrich. Hexane (98.25%), acetone (99.98%), methanol (99.99%), and toluene (99.99%) were purchased from the Fischer Scientific. All chemicals were used as received.

**PbS CQD Synthesis.** The synthesis of 1.3 eV PbS CQDs was adapted from the procedure developed by Hines and Scholes,<sup>40</sup> and was performed under inert conditions using standard Schlenk line techniques. Details of synthesis are described in the Supporting Information.

**PbS/CdS Core/Shell CQD Synthesis.** The synthesis of PbS/CdS core/shell CQD is adapted, with modifications, from the procedure developed by M. S. Neo et al.<sup>31</sup> To prepare 0.1 nm (one monolayer) CdS shell-thick PbS/CdS core/shell CQD, we mixed 0.395 mL of ODE, 0.115 mL of OA, and 0.030 g of Cd(Ac)<sub>2</sub> in a 25 mL three-neck flask, connected to a Schlenk line assembly. The mixture was heated and stirred continuously under a vacuum at 100 °C for at least 1 h, forming a clear cadmium-oleate solution. The temperature was then reduced to 80 °C and the vacuum environment was swapped to an argon atmosphere. Two milliliters of the prepared PbS 50 mg/mL solution was swiftly injected into the flask and allowed to react under stirring for 10 min. The heating was then turned off and the reaction was quenched by adding 5 mL of cold hexane and the resultant solution was then added to 30 mL of acetone to precipitate out the CQDs. The same washing step for PbS CQDs was applied and the prepared CQDs were redissolved in toluene to a concentration of 50 mg/mL. Details of the conditions used to vary the CdS shell thickness are described in the Supporting Information.

**ZnO Nanoparticle Colloidal Solution Synthesis.** ZnO nanoparticles were synthesized using the method adapted from Pacholski et al. as described elsewhere.<sup>41</sup>

**Fabrication of Solar Cell Devices.** PbS and PbS/CdS CQD films were deposited using a layer-by-layer spin-coating process with an in situ solid-state ligand exchange process, carried out in an ambient atmosphere. Substrates were prepared by prepatterning ITO on glass, spin coating a layer of PEDOT:PSS at 5000 rpm and then annealing at 150 °C for at least 5 min before use. For each layer, a drop of CQD solution (50 mg/mL in toluene) was deposited onto the spinning substrate, with a spin rate of 2000 rpm, followed by two drops of 1% v/v EDT in methanol. While spinning, 3 drops of methanol were added followed by 3 drops of toluene to wash off unbound ligands and CQDs. This cycle was repeated to build up to the required thickness. In our study, all samples were standardized to have 6 layers of CQD deposited, which gave a thickness of about 150 ± 17 nm as measured by surface profilometry. Finally, the *n*-type layer was deposited by spin-coating ZnO colloidal solution on top of the as-prepared film at 1000 rpm and postdeposition annealing was not required.

In the halide treatment approach, solid-state ligand exchange was performed by covering the surface of PbS/CdS film with saturated CdCl<sub>2</sub> in methanol for Cl exchange and 10 mg/mL CTAB in methanol for Br exchange, over a period of 1 min. The sample was then spun dry at 2000 rpm before 3 drops of methanol were added to wash off excess halide ligands. For each layer of PbS/CdS CQD deposited, this procedure was repeated three times before the next layer was deposited, so as to ensure comprehensive ligand exchange.

In the hybrid ligand exchange approach, the same flooding procedure is followed as above but was carried out once instead of three times for each PbS/CdS layer. After 1 min of the halide treatment, the sample was spun dry and 3 drops of methanol were added. While spinning, this procedure was followed by one drop of 1% v/v EDT in methanol and then 3 drops of methanol and 3 drops of toluene. This completes one layer of PbS/CdS CQD film for the hybrid ligand exchange approach.

Finally top electrodes were formed by depositing aluminum by thermal evaporation in an Edwards 306 evaporator at  $1 \times 10^{-6}$  Torr to a thickness of 100 nm, with an evaporation rate of 0.1 nm/s. A shadow mask was used to pattern the electrodes.

**Morphological and Structural Characterization of CQD.** A morphological study of CQDs was performed using a JEOL 2010 transmission electron microscope (TEM), with EDX capability, operating at 200 kV and the Oxford JEOL 2200MCO aberration corrected, monochromated FEG-TEM operating at 80 kV. The mean particle sizes were fitted with a Gaussian distribution curve to the experimental size histogram. TEM samples were prepared by making dilute solutions of CQD, then briefly dipping the TEM grids into the solution and letting them dry in ambient conditions. For powder X-ray diffraction (Philips theta/2theta), samples were prepared by drop casting PbS or PbS/CdS CQD solutions onto glass.

**XRD Simulation.** Simulated XRD patterns were calculated using a modified procedure described elsewhere.<sup>42</sup> In outline, a core/shell atomistic model was built by simulating the epitaxial growth of a CdS zinc blende shell around PbS core with a rock salt structure using the common simple cubic positions of the rock salt and zinc blende crystal structure. Although the core diameter and shell thickness varied, the overall diameter of the core/shell particle was kept constant at 3.2 nm. Strain was incorporated into the atomistic model through continuum elasticity in a core/shell spherical geometry previously described.<sup>42,43</sup>

The XRD pattern of the atomistic model was then simulated from the Debye equation for kinematic diffraction using the program "DISCUS"<sup>44</sup> for a Cu K<sub>α</sub> X-ray source and accounting for the thermal dependence of the scattering with Debye-Waller factors. Instrument broadening was not considered in the simulations. The parameters used for the simulation are given in the Supporting Information

**Optical Characterization of CQD.** Optical absorption spectroscopy of the CQDs was measured on a Cary Varian 4000 UV-vis-NIR spectrophotometer with diluted CQD solution in a quartz cuvette. Steady-state photoluminescence (PL) measurements were taken using an automated spectrofluorometer (Fluorolog, Horiba Jobin-Yvon), with a 450 W xenon lamp excitation source and an InGaAs NIR detector. The excitation wavelength was 500 nm. All spectra were corrected for instrumental response using a calibration lamp of known emissivity. Time-resolved PL measurements were acquired using a time-correlated single photon counting (TCSPC) apparatus (Fluo-Time 300, PicoQuant GmbH). Film samples were photoexcited using a 507 nm laser head (LDH-P-C-510, PicoQuant GmbH) pulsed at 300 kHz (for PbS-OA and PbS/CdS-OA samples) or 8 MHz, with a pulse duration of 117 ps and fluence of ~0.5 μJ/cm<sup>2</sup>. The PL at the peak emission (~1100 nm) was collected using a high resolution monochromator and NIR-PMT detector assembly (H10330A-45, Hamamatsu). Mono or biexponential fits to the data were carried out using commercial fitting software (FluoFit v4.5.3, PicoQuant GmbH). CQD films were prepared on PEDOT:PSS-coated glass, with and without a ZnO top coat.

**Device Characterization.** All devices were loaded into a sealed testing chamber flushed with N<sub>2</sub> to minimize sample degradation. All devices were loaded into a sealed testing chamber and continuously purged with N<sub>2</sub> through testing to minimize photothermal

degradation.<sup>45</sup> Current–voltage ( $I$ – $V$ ) measurement was performed using a Keithley 2400 Source Meter. The voltage was swept from  $-0.5$  to  $1.0$  V at a step size of  $0.025$  V. AM1.5 solar spectrum illumination was produced by a Newport solar simulator fitted with an AM1.5 filter. The power density of the light source was calibrated with a Thorlabs D3MM thermal sensor.

## RESULTS AND DISCUSSION

**Synthesis and Characterization of Core/Shell PbS/CdS.** With a low-temperature cation-exchange method, we have been able to synthesize PbS/CdS core/shell CQD from  $1.3$  eV PbS CQD using the method reported by Neo et al.<sup>31</sup> The choice of a cation-exchange approach to produce core/shell nanocrystals as opposed to conventional repeated hot injection methods is important as it uses a relatively low temperature that minimizes the effect of Ostwald ripening, which would otherwise increase the size distribution.<sup>46</sup> A key feature is that the anionic framework of the CQD is preserved and the incoming cation is incorporated into a similar crystal structure.<sup>47</sup> CdS has a similar lattice constant to PbS and the ability to form a face-centered cubic (FCC) structure and thus, using CdS as a shell layer via cation exchange reduces strain-related defects that negate the benefits of a passivating shell layer. A unique feature of this technique is that the synthesized PbS/CdS core/shell colloidal quantum dots preserve the initial diameter of the original PbS CQD, whereas the PbS core decreases in size during the shell formation. The thickness of the CdS shell is hence governed by the concentration of the Cd source added for cation-exchange as described in the methods section and in the Supporting Information.

In addition, an energy-dispersive X-ray spectroscopy (EDX) and a simulation study done by Zhao et al.<sup>29</sup> backed the formation of a pure phase CdS shell rather than an alloyed Cd and Pb sulfide when PbS/CdS core/shell CQD are formed by the cation-exchange method.

The preservation of the overall CQD diameter is supported by TEM images (size distribution statistics are shown in Figure 1) while the reduction in PbS core diameter is reflected by a blueshift in the excitonic peak as shown in Figure 2. The core diameter and the shell thickness has been estimated using the empirical relationship of the PbS CQD size to its band gap as proposed by Moreels et al.<sup>48</sup>

$$E_g = 0.41 + (0.0252d^2 + 0.283d)^{-1} \quad (1)$$

where  $E_g$  is the band gap of the PbS CQD as determined by the excitonic peak feature in the absorption spectrum and  $d$  is the diameter of particle in nm. From the crystal structure of CdS (zinc blende), a good gauge of the thickness of a monolayer of CdS would be the nearest cadmium to sulfur atom distance, which is about  $0.25$  nm.<sup>49</sup> Our thinnest CdS shell thickness for the core/shell CQD was calculated to be  $0.1$  nm, using the band gap approach. Similar submonolayer CdS has been deduced in other work using this approach.<sup>50</sup> This discrepancy might be due to the fact that the thickness of shell layer is determined by subtracting the total CQD diameter from the diameter of the PbS core, which is only an estimation using the excitonic peak feature, and eq 1 assumes a spherical shaped-CQD. Furthermore, the PbS core has a common shared outer layer of sulfur atoms with the CdS layer. Thus, a simple subtraction of diameters may result in an apparent submonolayer value of CdS.

Because of the similarity in crystal structure and lattice constant of CdS and PbS, it is difficult to image the thin layer of

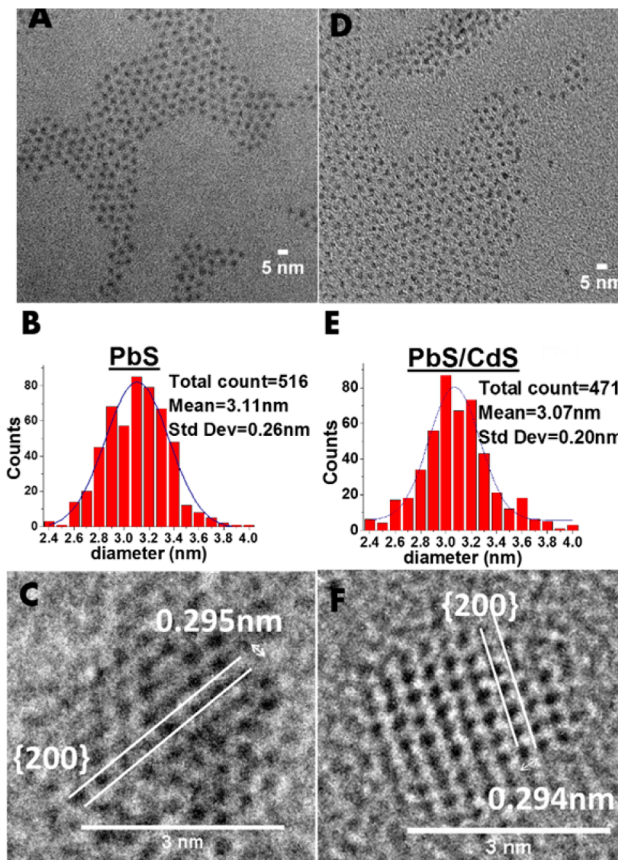


**Figure 1.** TEM images of PbS and PbS/CdS core/shell CQDs. (a, d) Low-magnification images of  $1.26$  eV PbS CQD and  $1.34$  eV PbS/CdS CQD, respectively. PbS/CdS CQDs have a calculated  $0.1$  nm CdS shell and is synthesized from the same batch as the PbS CQDs. (b, e) Histograms of the size distribution, with a Gaussian fit, of  $1.26$  eV PbS CQDs and  $1.34$  eV PbS/CdS CQDs, respectively. (c, f) High-magnification images of  $1.26$  eV PbS CQD and  $1.34$  eV PbS/CdS CQD, respectively.

CdS using high-resolution TEM.<sup>51</sup> However, evidence for an epitaxial CdS shell can be determined using XRD. The presence of an increasing CdS phase composition with increasing CdS shell thickness implies that the CdS only exists as part of the core/shell heterostructure and, eliminating the possibility of the nucleation of separate CdS phases and homogeneous alloying. As illustrated in Figure 3a, the relative peak heights of the PbS/CdS core/shell CQD sample and positions are influenced by the CdS shell on the PbS core. Taking the most obvious peaks as an example, pure bulk CdS zinc blende has a higher peak intensity for the  $\{111\}$  reflections compared to the  $\{200\}$  reflections whereas both PbS CQD and pure PbS bulk phase (rocksalt structure) have almost equal intensities for these reflections. For a core/shell structure with a constant diameter, a thicker shell layer would increase its overall composition with respect to the amount of PbS left in this heterostructure. This model is consistent with our XRD results, showing an increasing  $\{111\}$  intensity while the  $\{200\}$  peak decreases as the CdS shell thickness increases. In addition, Figure S1 in the Supporting Information excludes the possibility of a hexagonal phase of CdS. These observations are also supported by the work of Zhao et al., who demonstrate that if an alloyed  $Pb_xCd_{1-x}S$  phase shell is formed then a much smaller band gap would be observed.<sup>29</sup>

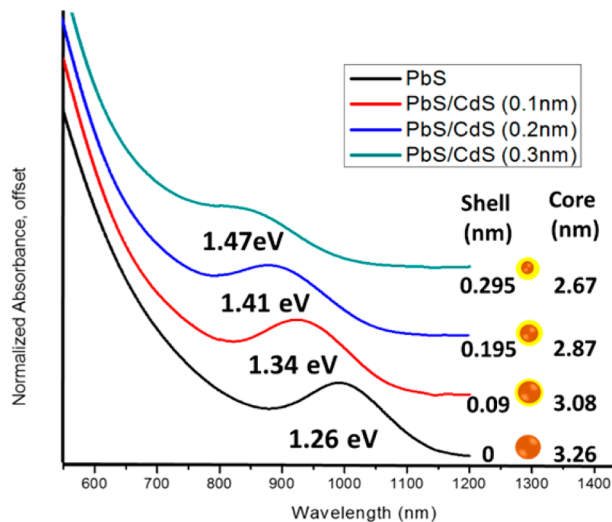


**Figure 2.** Normalized absorbance curve of PbS CQDs and PbS/CdS CQDs with increasing shell thickness, synthesized from the same PbS batch. Absorption was carried out with CQDs dissolved in toluene with oleic acid as ligands. The schematic inset serves as a visual aid, displaying the calculated shell thickness and core diameter displayed. A systematic blueshift of peaks with thicker shell layer implies a decrease in PbS core diameter.

Our observation is supported by XRD simulations as illustrated in Figure 3b, which is based on an atomistic model of PbS/CdS rock salt/zinc blende core/shell nanoparticle using the Debye equation for kinematic diffraction.<sup>52</sup> The transition of peak heights from PbS to CdS reveals the close proximity of the core and shell atoms, causing the scattered X-rays to constructively interfere between the two materials giving rise to a perceived average of the two diffraction patterns. Quantitative analysis using EDX on TEM samples indicates not only the presence of cadmium, but yields an atomic composition as that in PbS/CdS core/shell CQDs with a 0.1 nm CdS shell (see the Supporting Information, Figure S2). Raman spectra (see the Supporting Information, Figure S3) also indicates the presence of CdS and shows that the CdS peaks are slightly red-shifted. This latter observation is consistent with the effect of a material under tensile strain, which is expected for CdS epitaxially grown on the surface of PbS. At this juncture, it is important to note that this cationic exchange approach differs from the hybrid passivation scheme developed by Ip et al., which utilizes a long-chain phosphonic acid molecule to selectively deliver cadmium cations to the PbS surface site. They observed no obvious change in excitonic absorption peak wavelength and showed, using X-ray photoelectron spectroscopy (XPS), an atomic ratio of Pb to Cd atom of 1 to less than 0.05.<sup>21</sup> However, in our study, we observed a sizable blueshift in absorbance peak and EDX results backing up theoretical composition calculations of 1 Pb to 0.25 Cd atoms. Together with the observations that there is no separate CdS evident in TEM images and that the band gap increases with no apparent decrease in CQD size, we conclude that an epitaxial CdS shell forms on the PbS core.

**Incorporation of PbS/CdS CQD into Devices.** The PbS/CdS core/shell quantum dots have been used to form the p-type layer of a heterojunction device as shown in Figure 4a with the full procedure described in the methods section. It should be noted that all PbS/CdS CQD were derived from the same batch of PbS. Briefly, each layer of CQD film was formed by spin coating followed by a solid state ligand exchange with a

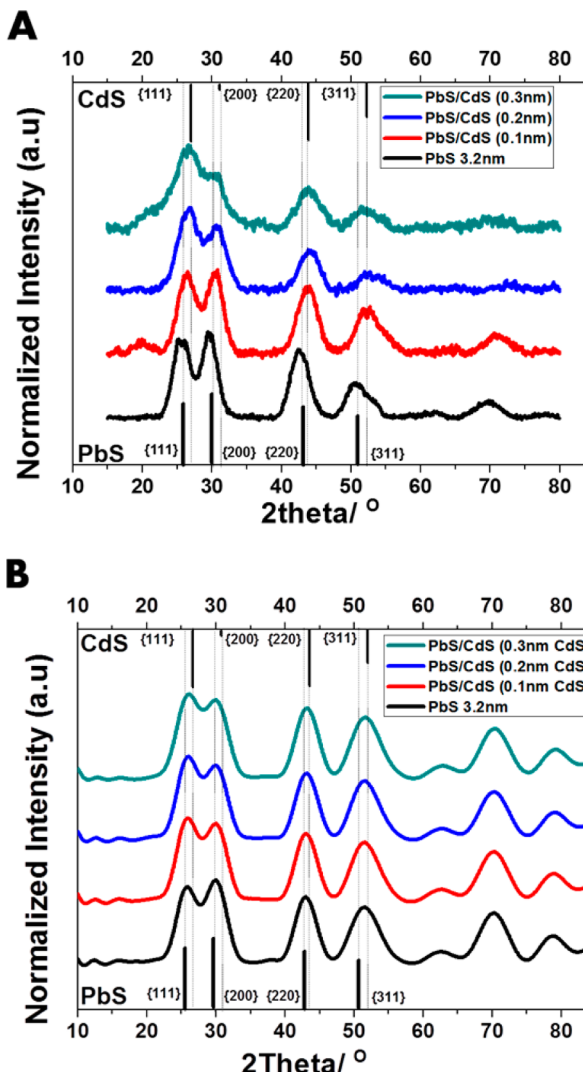


**Figure 3.** (a) Experimental X-ray diffraction patterns of PbS and PbS/CdS CQDs drop cast on glass substrates. PbS and CdS peaks are referenced from JCPDS file 01-078-1057 and 00-001-0647, respectively. Main peaks of both PbS and CdS phases are labeled and guidelines to peaks are drawn to highlight the subtle shifts in peak position and relative intensity from PbS to CdS with increasing CdS shell thickness. (b) Simulated X-ray diffraction pattern of PbS and PbS/CdS CQD with varying shell thicknesses with an overall diameter of 3.2 nm.

bifunctional linker molecule, 1,2-ethanedithiol (EDT). Each test device consisted of 6 layers of CQD films, which gives an overall layer thickness of  $150 \pm 18$  nm as measured by surface profilometry, which are then capped with colloidal ZnO to a thickness of  $100 \pm 24$  nm, without any postdeposition anneal treatment. This test device architecture is kept consistent throughout this study. We performed photovoltaic performance testing under AM 1.5 illumination and we first compare devices made using PbS and PbS/CdS with 0.1 nm shell thickness. The current density–voltage ( $J-V$ ) characteristic curves in Figure 4b reveal that although the short-circuit current ( $J_{SC}$ ) is substantially lower for the PbS/CdS device,  $V_{OC}$  exceeds that of the nonshelled PbS device by more than 0.2 V.

A PbS band gap change of 0.08 eV from 1.26 to 1.34 eV (as would be predicted using the method of Yoon et al.,<sup>19</sup> in this work moving from a PbS to a PbS/CdS CQD with 0.1 nm shell

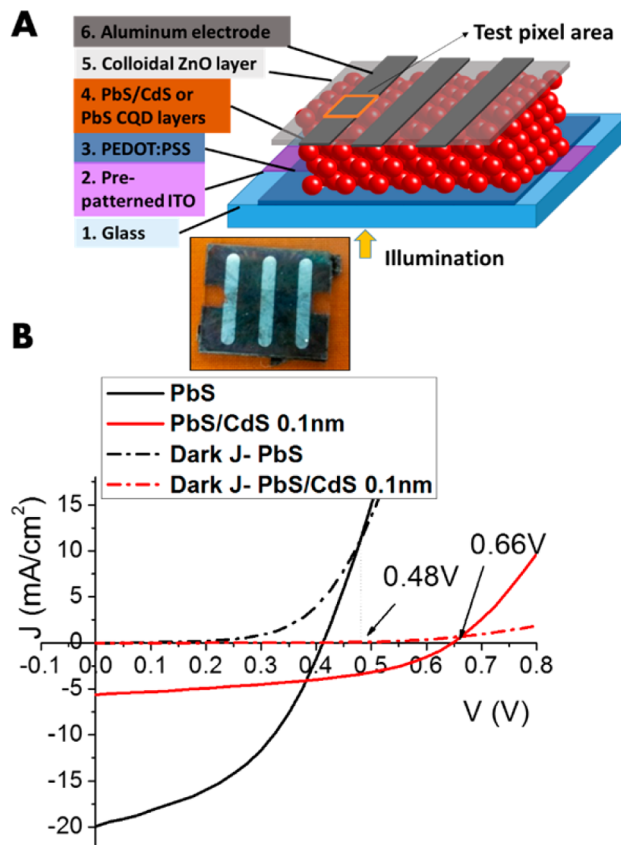


**Figure 4.** (a) Model showing the device architecture of the solar cell used for performance testing. Inset shows the actual sample device. (b) Current density versus voltage performance testing of best performing devices under dark and AM1.5 illumination conditions. Both devices have the same structure, with similar thickness and underwent the same solid-state ligand exchange process using EDT. Arrows indicate the voltage points where light generated current equals the dark current and gives an estimate of the built in potential of the device. Refer to Table 1 for a summary of the average performance statistics.

thickness) would result in only a 0.044 V change in  $V_{OC}$  if it were due only to an increase in band offset. Hence, the greater increase of  $V_{OC}$  observed must be due to additional factors. Using dark and illuminated  $J-V$  curves to estimate the built-in potential and comparing it with  $V_{OC}$ , it is clear that the PbS devices suffer a greater voltage loss than the PbS/CdS devices, as shown in Figure 4b. Zhao et al.<sup>53</sup> have reported a similar improvement in  $V_{OC}$  resulting from a postdeposition annealing treatment of a PbS CQD film, which forms a thin layer of oxide on the surface of PbS. We postulate that the thin CdS shell layer effectively passivates surface defects of the PbS core because cation-exchange relies on the replacement of the original host cationic species resulting in the complete bonding of every PbS surface atom. Therefore, deleterious deep traps that promote nonradiative recombination are minimized and this gives a rise in  $V_{OC}$ .<sup>9</sup> To confirm that the improvement in  $V_{OC}$  originates from the core/shell passivation strategy, we tested a set of CQD devices fabricated using an aluminum metal Schottky junction instead of ZnO. Results from these show that even without a p-n junction that shell passivation is effective (see the Supporting Information, Figure S4).

**Effect of Shell Thickness and Passivation.** To maximize the benefit of shell passivation, in the context of solar cell devices, the shell thickness has to be optimized such that it is

sufficiently thick for complete passivation, yet sufficiently thin for charges to be transported dot to dot. Using the same starting core PbS CQD, a series of core/shell CQDs with increasing shell thicknesses were examined using the same procedure. Figure 5 shows four device performance metrics that

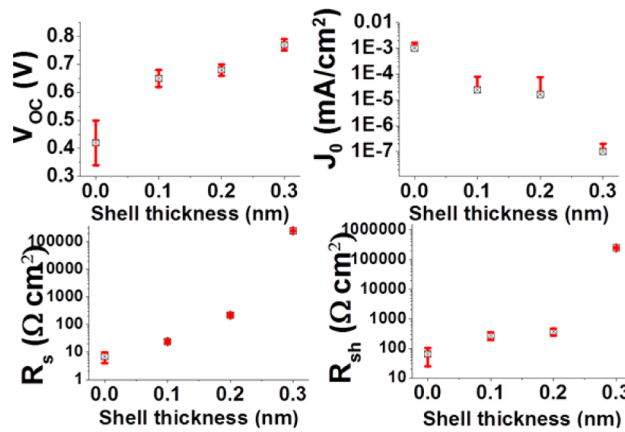


**Figure 5.** (a) Open circuit voltage, (b) reverse saturation current, (c) series resistance, (d) shunt resistance versus thickness of CdS shell layer on PbS/CdS core/shell CQDs. 0 nm shell thickness refers to unshelled PbS CQD and all PbS/CdS CQDs are synthesized from the same batch of PbS. Devices have the structure shown in Figure 4a.

demonstrate the effect of shell passivation and  $J-V$  curves versus shell thickness are illustrated in Figure S5 in the Supporting Information.

These experiments show an increase in  $V_{OC}$  with increasing shell thickness, with the most substantial change between no shell and a 0.1 nm shell. Ip et al.<sup>21</sup> showed that a reduction of surface related trap density increases  $V_{OC}$  by exploring the effect of midgap trap states using density functional theory simulations. It is most likely, that at 0.1 nm shell thickness, surface passivation is complete, i.e., each PbS core surface atom is fully bonded. Thus, additional layers do not lead to a substantial increase in passivation and the subsequent rise in  $V_{OC}$  is small and attributed to the increase in band gap due to the decrease in PbS core diameter.<sup>19</sup>

To investigate carrier recombination characteristics, we have measured the shunt resistance ( $R_{sh}$ ) and the reverse saturation current ( $J_0$ ) of our devices.  $J_0$  is a direct measure of recombination, whereas  $R_{sh}$  measures the amount of photocurrent leakage when the cell is under load, which is in part due to recombination of charges. Thus, the better the passivation of defects, the lower the recombination current and hence  $J_0$  should decrease, whereas shunt resistance should increase. As shell thickness increases we observe that  $J_0$  and  $J_{sc}$  decrease while  $R_s$  and  $R_{sh}$  increase. This can be attributed to a reduction in overall charge transport due to a larger tunneling barrier forming between CQD, resulting in reduced delocalization of electronic wave functions.<sup>37</sup>

Passivation of defect states can also lead to a lower carrier concentration as the CQD becomes more intrinsic in nature, thereby reducing conductivity and hence increasing the overall series resistance.<sup>53</sup> It has also been reported that cation-exchange tends to be less uniform when thicker shells are formed, i.e. shell growth may be preferential at a certain crystal facet, giving rise to a broader excitonic peak<sup>29</sup> as observed in Figure 2, and this could be detrimental to device performance.<sup>54</sup> Core/shell CQDs with CdS shells less than 0.1 nm were

also synthesized and evaluated as possible solar cell devices but gave no distinct improvement to  $V_{OC}$ . Therefore, we conclude that 0.1 nm CdS shell is the thinnest shell layer that can achieve sufficient surface passivation, which is regarded as optimal and further investigation was carried out using this particular core/shell PbS/CdS size.

To further understand the nature of passivation provided by a shell material with a larger band gap, we have both steady-state and time-resolved photoluminescence (Figures 6a, b). Photoluminescence yield in this study is not absolute but can be used comparatively across the sample sets because they are all prepared in a similar fashion with approximately the same thickness of CQD layer following the approach used by

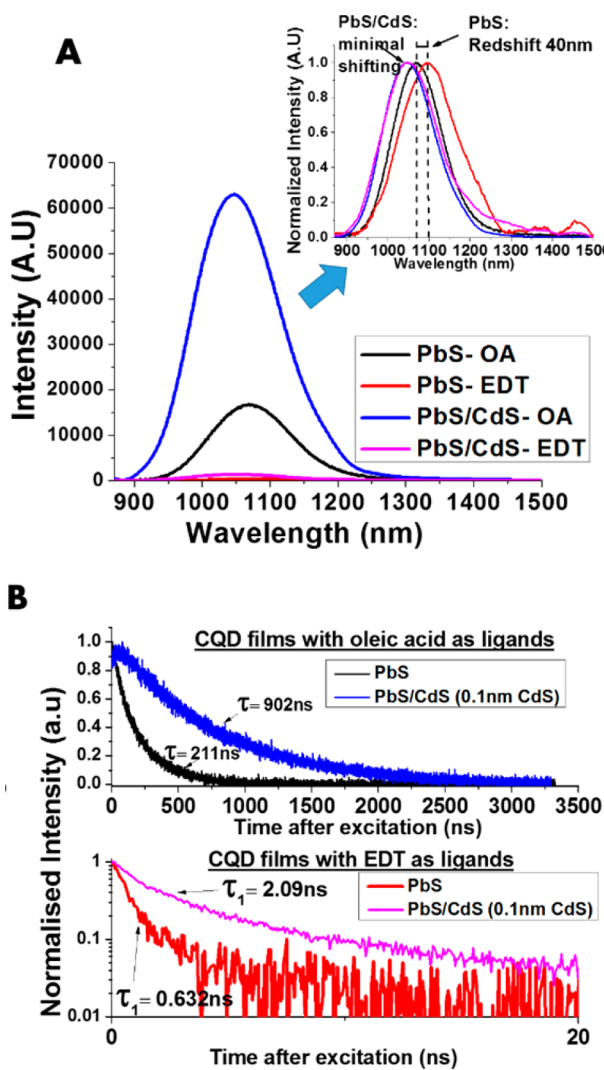


**Figure 6.** (a) Photoluminescence spectra of CQD films, showing significantly higher photoluminescence intensity of core/shell CQDs and the quenching effects of ligand exchange from OA to EDT. Inset shows the normalized intensity of the curves illustrating the extent of redshift of the photoluminescence peaks. (b) Photoluminescence decay curves of the same samples described in a. Detection wavelength for each decay curve is based on the peak emission shown in a. The fitted decay time constants are displayed alongside the graphs and are based on monoexponential decay for OA samples. For EDT samples, fitting is based on biexponential decay and the faster decay time constant is displayed as  $\tau_1$ . The corresponding  $\tau_2$  is 7.45 and 15.97 ns for PbS and PbS/CdS, respectively.

Pietryga et al.<sup>30</sup> The effect of shell passivation manifests in two ways:

(1) Passivation should lead to a reduction in trap states, especially deep traps, which are responsible for nonradiative recombination.<sup>21</sup> This is directly reflected in radiative recombination by an increase in photoluminescence intensity for the core/shell sample compared to a core-only CQD sample. Furthermore, for both oleic acid (OA) and EDT as ligands, core/shell CQDs display much longer decay lifetimes, typically 3–4 times longer than core-only PbS (Figure 6b and the Supporting Information, Figure S6). A prolonged excitonic lifetime is an indicator that the faster, nonradiative, recombination channels are suppressed.

(2) The addition of a CdS shell enhances the quantum confinement effect (both carriers for type I), therefore buffering the effects of surface chemistry changes. When OA is replaced by EDT, a small bifunctional ligand, which is known to physically link and energetically couple neighboring CQDs, the overlap of their wave functions is enhanced, resulting in a relaxation of charge carrier confinement.<sup>26</sup> This results in a lower energy first excitonic transition, which is observed as a redshift in the exciton peak of the absorption or photoluminescence spectra.<sup>55,56</sup> However, when PbS CQD are overcoated with a CdS shell, the extent of emission peak redshift is lower, as shown in Figure 6a.

In light of these findings, we can surmise that employing a CdS shell not only acts as a surface trap passivation strategy but also buffers the PbS core electronic states from changes in the surface states because of ligand exchange. The benefits of having a passivating CdS shell is illustrated in the band diagrams shown in Figure 7a. The alignment and the subsequent band bending at the PbS–ZnO interface results in electron injection from PbS CQD into ZnO conduction band. Charge carriers could be lost through recombination via traps caused by surface defects interquantum dot interfaces. Therefore, employing core/shell PbS/CdS CQDs may well be an important step forward in addressing the problems caused by incomplete passivation or ligand instability, which are thought to be the main source of surface defects in quantum dot solar cells.

**Relaxation of the Charge Transport Barrier Imposed by the Shell Layer.** Our preliminary results (Figure 4b) reveal that shell passivation comes at the price of lowering charge transport capacity as shown by the lower overall photocurrent harnessed and the greater series resistance. Charges now have to tunnel through both the shell and the ligand matrix to neighboring CQDs to get to their respective electrodes. EDT, being a bifunctional linker, draws the CQDs closer together and enhances coupling between the quantum dots.<sup>26</sup> However, even with EDT ligands, our observation from photoluminescence studies imply that energetic coupling among core/shell CQDs is less significant compared to their nonshelled counterparts as shown by the minimal redshift of the photoluminescence emission peak. Therefore, to improve charge transport in an array of core/shell CQDs it is necessary to further decrease interdot distance or to relax the confinement potential of CdS shell by changing its surface chemistry.

Recently, two new classes of inorganic ligands have been reported to produce CQD films with high carrier mobility, namely metal chalcogenide complexes<sup>57,58</sup> and small molecular<sup>59,60</sup> or atomic ligands.<sup>61–63</sup> Here, we investigate halide atomic ligands since they have recently been shown to increase the efficiency of PbS CQD devices.<sup>64</sup> The use of these halide

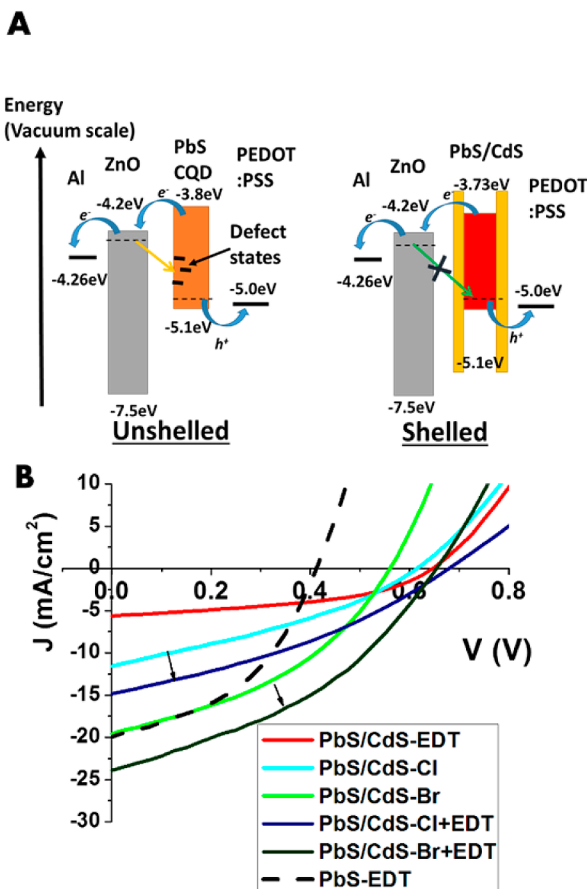


**Figure 7.** (a) Schematic diagram showing the proposed band alignment of the heterojunction cell and the defect mediation effect of a CdS shell on the PbS electronic structure. Defect states promotes nonradiative recombination when charges moves between CQDs or between PbS and ZnO interface. Adding a CdS shell reduces recombination, thus improving  $V_{OC}$ . (b) Current density versus voltage performance testing of the best PbS/CdS devices formed from different ligand exchange treatments with a PbS device performance shown as reference. Arrows highlight the improvement of hybrid treatment over standalone halide treatment for ligand exchange. Refer to Table 1 for the device performance statistics.

ligands requires a cadmium cation and a long chain phosphonic acid molecule conjugation to deliver the halide ligand to the PbS surface. It was noted through absorption studies that a

complete cadmium shell is not formed as cadmium binds only to exposed sulfur atoms and the rest of the exposed lead atoms are bonded to the halide atoms. These methods gave record efficiency CQD solar cell devices at the time of publication and results were attributed to effective passivation and increased carrier mobility.<sup>64</sup>

Tang et al. have also shown that different halide ligands gave different mobility results with the trend being that mobility increases from chlorine, through bromine to iodine. Interestingly, more recent studies have shown that when halide treatment was performed on PbS without cadmium, PbS with n-type character is produced.<sup>27</sup> With cadmium incorporation, the formation of donor states seems to be suppressed, whereas carrier mobility is improved, in similar fashion to atomic ligand passivation.<sup>64</sup> From this, we hypothesized that with a cadmium sulfide layer on PbS for our core/shell CQD, there could be a similar effect of improving carrier mobility while minimizing the chances of introducing donor states in the PbS band structure.

To maximize device performance, we carried out a halide surface treatment,<sup>21,64</sup> using cadmium chloride ( $CdCl_2$ ) for chlorine (Cl) source and cetyltrimethylammonium bromide (CTAB) for the bromine (Br) source, on our PbS/CdS (0.1 nm CdS shell) CQD films. The performance of the devices with halide ligand exchange demonstrates an improvement in efficiency. Figure 7b shows that there is a major improvement in current density for both halides treatment but  $V_{OC}$  shows a decrease from the reference EDT-passivated PbS/CdS device. It is evident that the increase in  $J_{SC}$  for a CTAB treatment is higher than that for  $CdCl_2$  and accordingly the drop in  $V_{OC}$  is more significant. The improvement in  $J_{SC}$  improvement is consistent with the mobility studies performed by Tang et al. for different halide passivation where Br gives higher mobility than Cl, improving charge transport and leading to overall increase in extracted photocurrent.

To further improve charge transport, we seek to exploit the linking properties of EDT and to use it in conjunction with halide treatment. Ip et al. have reported that the average spacing between quantum dots is much smaller when organic bifunctional linkers are used as compared to purely inorganic halide ligands.<sup>21</sup> We also note that despite similar film thicknesses, our halide treated films look optically less dense than EDT treated films. While thiols, such as EDT, provide good surface passivation,<sup>65,66</sup> together with the passivation provided by the CdS shell, carrier mobility would be hampered. Thus, we propose that optimizing the performance of the CQD

**Table 1. Performance Data for Heterojunction CQD Solar Cells (ITO/PEDOT:PSS/CQDs/ZnO/Al) under AM 1.5 Spectral Illumination (100 mW/cm<sup>2</sup>)<sup>a</sup>**

	ligand	$J_{sc}$ (mA/cm <sup>2</sup> )	$V_{oc}$ (V)	FF	PCE (%)	$J_o$ (mA/cm <sup>2</sup> )	$R_s$ ( $\Omega$ cm <sup>2</sup> )	$R_{sh}$ ( $\Omega$ cm <sup>2</sup> )
PbS	EDT	$17.9 \pm 3.5$ (19.8)	$0.41 \pm 0.09$ (0.42)	$0.45 \pm 0.06$ (0.44)	$3.40 \pm 0.22$ (3.66)	$(1.2 \pm 0.7) \times 10^{-3}$	$6.52 \pm 0.93$	$55.5 \pm 14.2$
PbS/ CdS	EDT	$5.9 \pm 1.4$ (6.2)	$0.65 \pm 0.04$ (0.65)	$0.42 \pm 0.06$ (0.42)	$1.37 \pm 0.28$ (1.69)	$(1.3 \pm 0.3) \times 10^{-5}$	$23.9 \pm 4.3$	$324 \pm 14$
	Cl	$11.2 \pm 2.3$ (11.8)	$0.63 \pm 0.03$ (0.61)	$0.33 \pm 0.04$ (0.33)	$2.16 \pm 0.14$ (2.38)	$(6.3 \pm 0.4) \times 10^{-5}$	$23.6 \pm 3.5$	$69.9 \pm 6.3$
	Br	$17.4 \pm 1.2$ (19.4)	$0.54 \pm 0.04$ (0.55)	$0.39 \pm 0.02$ (0.39)	$3.83 \pm 0.30$ (4.16)	$(5.0 \pm 0.4) \times 10^{-4}$	$10.1 \pm 2.4$	$61.0 \pm 4.8$
	Cl +EDT	$13.8 \pm 1.9$ (14.8)	$0.66 \pm 0.03$ (0.68)	$0.34 \pm 0.03$ (0.34)	$3.12 \pm 0.22$ (3.42)	$(9.4 \pm 0.5) \times 10^{-5}$	$24.9 \pm 3.3$	$76.2 \pm 5.4$
Br +EDT	Br +EDT	$21.9 \pm 2.4$ (23.9)	$0.63 \pm 0.04$ (0.65)	$0.38 \pm 0.03$ (0.39)	$5.61 \pm 0.38$ (6.05)	$(2.0 \pm 0.4) \times 10^{-4}$	$11.8 \pm 2.6$	$58.1 \pm 3.9$

<sup>a</sup>PbS/CdS CQD is with 0.1 nm CdS shell. Results are averaged with standard deviation across 12 samples on 4 different substrates. The  $J_{sc}$   $V_{oc}$ , FF, and PCE of champion devices are quoted in brackets.

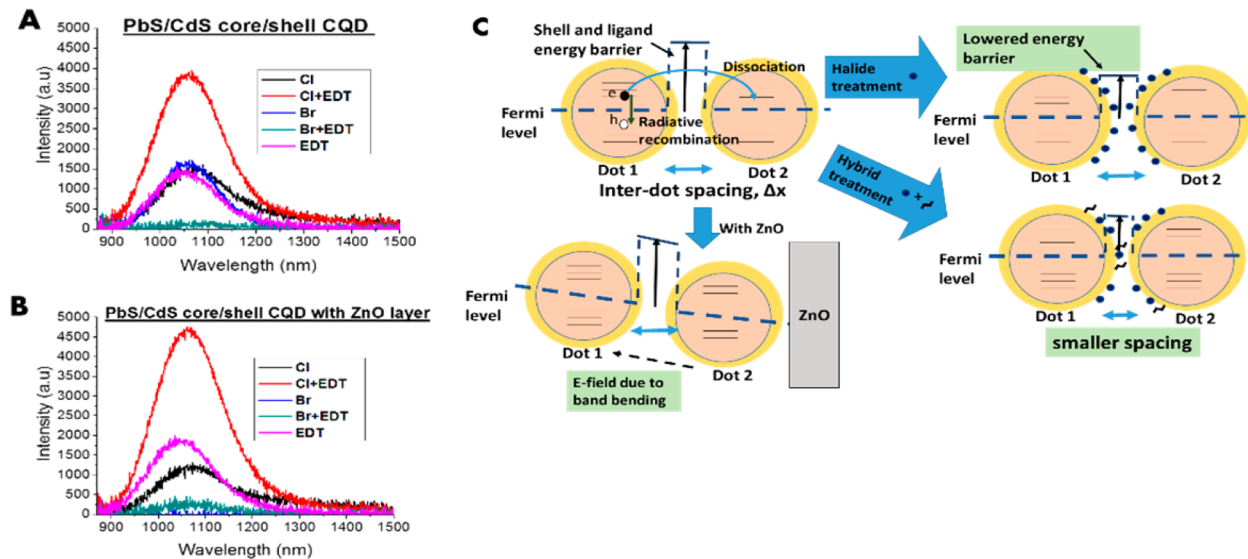


**Figure 8.** (a) Photoluminescence spectra of CQD films, prepared with similar thicknesses, after halide or hybrid ligand treatment. (b) Photoluminescence spectra of CQD films prepared in the same way as (a) but with an extra layer of *n*-type ZnO deposited (as in test device fabrication) (c) Schematic diagram illustrating the competing effect between radiative recombination and electron–hole pair dissociation. Dissociation is aided by a lowering of energy barrier for transport, the reduction of interparticle spacing and also the band bending effect resulting from a heterojunction formation.

film requires a balance of mobility improvement and passivation. Mobility is improved by introducing halide ligands and can be used together with EDT that decreases the separation of the CQDs.

We carried out our hybrid treatment by reducing the ligand exchange time for halide treatment to only one cycle to avoid total replacement with halide ligands and then used EDT to swap out the remaining oleic acid ligands. Results in Figure 7a and Table 1 show the improvement when both halide and EDT ligands are used for passivation, with  $V_{OC}$  increased compared to a halide-only treatment with a concomitant increase in  $J_{SC}$ .

To investigate the effect of having both EDT and halide species as ligands, we employed photoluminescence studies. PbS films were produced on poly(3,4-ethylenedioxythiophene)-poly(styrenesulfonate) (PEDOT:PSS)-coated glass, with and without a ZnO top coat. Photoluminescence quenching is a useful measure for determining whether charge separation is occurring at an interface.<sup>67</sup> Steady-state spectra of our core/shell CQD films treated with the respective halides (Figure 8a) reveals no quenching and minimal redshift of the first exciton transition peak energy with reference to the EDT-treated sample. However, when a heterojunction is formed with the *n*-type ZnO, the photoluminescence spectra reveal quenching of photoluminescence peaks for both halide-treated films with greater quenching in the case of Br (Figure 8b). The heterojunction formation results in band bending, providing an internal electric field to drift the charge carriers thus aiding charge separation. In summary, our observations suggest that

- (1) The decrease in  $V_{OC}$  values obtained for halide-treated devices might be due a change in the surface chemistry of the CdS shell caused by halide ligands. This may lower the confinement effect, lowering the barrier to charge transport.
- (2) CTAB treatment has a greater effect on lowering the confinement barrier compared to  $CdCl_2$ , as reflected by the greater extent of photoluminescent quenching and larger decrease in  $V_{OC}$ .

Further EDX experiments reveals that  $CdCl_2$  treatment might have increase the CdS shell thickness slightly by increasing Cd composition, thereby enforcing passivation and minimizing the drop in  $V_{OC}$  (see Figure S7 in the Supporting Information).

For both Cl+EDT and Br+EDT hybrid treatment, energetic coupling should be more significant compared to EDT treatment alone due to the combined effect of closer interdot spacing and reduced quantum confinement brought about by halide ligands. This is indicated by a slight redshift of the photoluminescence peak, using the EDT treated sample peak as the reference, which is observed both with and without the ZnO layer (Figure 8a, b, respectively). However, photoluminescence quenching was not observed for hybrid treated samples when a ZnO layer was added, and instead a higher photoluminescence yield was recorded. This is also the case for EDT-only treated samples. The passivation brought about by EDT ligands may influence the radiative recombination rate, as it was shown to alter the valence band level in lead selenide nanocrystals when forming a heterojunction with ZnO.<sup>68</sup> However, further studies are needed to fully understand why photoluminescence quenching is not observed.

In summary, the addition of EDT with halide ligands improves passivation but also improves charge transport, giving rise to both improved  $V_{OC}$  and  $J_{SC}$  when compared to a bare halide treatment.

## CONCLUSIONS AND FUTURE OUTLOOK

The studies reported here have shown that by using PbS/CdS core/shell CQDs,  $V_{OC}$  can be enhanced and in conjunction with a combination of passivation strategies,  $J_{SC}$  can be held at a level that increases PV device efficiency. A CdS shell layer not only provides effective surface passivation but also buffers the core electronic energies from the surface chemistry. This resulted in improved  $V_{OC}$  at the expense of  $J_{SC}$ . To mitigate this we have showed that it is possible to alter the energy barrier imposed by the shell material by the use of halide ligands and

that the extent of passivation can be regulated by a synergistic use of both halide and bifunctional EDT ligands. Using this approach, we were able to boost the photocurrent without losing the effect of shell passivation and our best device demonstrated an impressive 6% power conversion efficiency. The device architecture presented here is comparatively simple and there is substantial capacity for further efficiency improvements with more complex architectures.

## ■ ASSOCIATED CONTENT

### Supporting Information

Details of PbS and PbS/CdS CQD synthesis, XRD simulation, EDX, Raman spectra, Schottky cells performance, and additional photoluminescence data. This material is available free of charge via the Internet at <http://pubs.acs.org>.

## ■ AUTHOR INFORMATION

### Corresponding Author

\*E-mail: andrew.watt@materials.ox.ac.uk. Tel: +44 1865 613455 or +44 7828 598301. Fax: +44 1865 273789.

### Author Contributions

<sup>‡</sup>The manuscript was written through contributions of all authors. All authors have given approval to the final version of the manuscript. These authors contributed equally.

### Funding

We acknowledge funding from EPSRC (Platform Grant EP/F048009/1)

### Notes

The authors declare no competing financial interest.

## ■ ACKNOWLEDGMENTS

D.C.J.N. thanks A\*STAR for an overseas research scholarship.

## ■ REFERENCES

- (1) Maenosono, S.; Okubo, T.; Yamaguchi, Y. *J. Nanoparticle Res.* **2003**, *5*, 5–15.
- (2) Tekin, E.; Smith, P. J.; Schubert, U. S. *Soft Matter* **2008**, *4*, 703.
- (3) Choi, K.-H.; Jeong, J.-A.; Kang, J.-W.; Kim, D.-G.; Kim, J. K.; Na, S.-I.; Kim, D.-Y.; Kim, S.-S.; Kim, H.-K. *Sol. Energy Mater. Sol. Cells* **2009**, *93*, 1248–1255.
- (4) Beard, M. C.; Luther, J. M.; Semonin, O. E.; Nozik, A. J. *Acc. Chem. Res.* **2013**, *46*, 1252–1260.
- (5) Nozik, A. J. *Nat. Photonics* **2012**, *6*, 272–273.
- (6) Wu, J.; Mangham, S. C.; Reddy, V. R.; Manasreh, M. O.; Weaver, B. D. *Sol. Energy Mater. Sol. Cells* **2012**, *102*, 44–49.
- (7) Hyeon-Deuk, K.; Prezhdoo, O. V. *J. Phys.: Condens. Matter* **2012**, *24*, 363201.
- (8) Pandey, A.; Guyot-Sionnest, P. *Science* **2008**, *322*, 929–932.
- (9) Talapin, D. V.; Lee, J.-S.; Kovalenko, M. V.; Shevchenko, E. V. *Chem. Rev.* **2010**, *110*, 389–458.
- (10) Lesnyak, V.; Gaponik, N.; Eychmüller, A. *Chem. Soc. Rev.* **2013**, *42*, 2905.
- (11) Semonin, O. E.; Luther, J. M.; Beard, M. C. *Mater. Today* **2012**, *15*, 508–515.
- (12) Hillhouse, H. W.; Beard, M. C. *Curr. Opin. Colloid Interface Sci.* **2009**, *14*, 245–259.
- (13) Kramer, I. J.; Sargent, E. H. *Chem. Rev.* **2013**, *130*, 920103133002.
- (14) Jeong, K. S.; Tang, J.; Liu, H.; Kim, J.; Schaefer, A. W.; Kemp, K.; Levina, L.; Wang, X.; Hoogland, S.; Debnath, R.; et al. *ACS Nano* **2012**, *6*, 89–99.
- (15) Ehrler, B.; Musselman, K. P.; Böhm, M. L.; Morgenstern, F. S. F.; Vaynzof, Y.; Walker, B. J.; MacManus-Driscoll, J. L.; Greenham, N. C. *ACS Nano* **2013**, *7*, 4210–4220.
- (16) Gao, J.; Jeong, S.; Lin, F.; Erslev, P. T.; Semonin, O. E.; Luther, J. M.; Beard, M. C. *Appl. Phys. Lett.* **2013**, *102*, 043506.
- (17) Klem, E. J. D.; Shukla, H.; Hinds, S.; MacNeil, D. D.; Levina, L.; Sargent, E. H. *Appl. Phys. Lett.* **2008**, *92*, 212105.
- (18) Fischer, A.; Rollny, L.; Pan, J.; Carey, G. H.; Thon, S. M.; Hoogland, S.; Voznyy, O.; Zhitomirsky, D.; Kim, J. Y.; Bakr, O. M.; et al. *Adv. Mater.* **2013**, *25*, 5742–5749.
- (19) Yoon, W.; Boercker, J. E.; Lumb, M. P.; Placencia, D.; Foos, E. E.; Tischler, J. G. Enhanced Open-Circuit Voltage of PbS Nanocrystal Quantum Dot Solar Cells. *Sci. Rep.* **2013**, *3*.
- (20) Bakulin, A. A.; Neutzner, S.; Bakker, H. J.; Ottaviani, L.; Barakel, D.; Chen, Z. *ACS Nano* **2013**, *7*, 8771–8779.
- (21) Ip, A. H.; Thon, S. M.; Hoogland, S.; Voznyy, O.; Zhitomirsky, D.; Debnath, R.; Levina, L.; Rollny, L. R.; Carey, G. H.; Fischer, A.; et al. *Nat. Nanotechnol.* **2012**, *7*, 577–582.
- (22) Liu, H.; Zhitomirsky, D.; Hoogland, S.; Tang, J.; Kramer, I. J.; Ning, Z.; Sargent, E. H. *Appl. Phys. Lett.* **2012**, *101*, 151112.
- (23) Ning, Z.; Zhitomirsky, D.; Adinolfi, V.; Sutherland, B.; Xu, J.; Voznyy, O.; Maraghechi, P.; Lan, X.; Hoogland, S.; Ren, Y.; et al. *Adv. Mater.* **2013**, *25*, 1719–1723.
- (24) Moreels, I.; Fritzinger, B.; Martins, J. C.; Hens, Z. *J. Am. Chem. Soc.* **2008**, *130*, 15081–15086.
- (25) Turyanska, L.; Elfurawi, U.; Li, M.; Fay, M. W.; Thomas, N. R.; Mann, S.; Blokland, J. H.; Christianen, P. C. M.; Patanè, A. *Nanotechnology* **2009**, *20*, 315604.
- (26) Law, M.; Luther, J. M.; Song, Q.; Hughes, B. K.; Perkins, C. L.; Nozik, A. J. *J. Am. Chem. Soc.* **2008**, *130*, 5974–5985.
- (27) Zhitomirsky, D.; Furukawa, M.; Tang, J.; Stadler, P.; Hoogland, S.; Voznyy, O.; Liu, H.; Sargent, E. H. N-Type Colloidal-Quantum-Dot Solids for Photovoltaics. *Adv. Mater.* **2012**, *24*.
- (28) Dai, N.; Chen, J. CdSe/ZnS Core/shell Quantum Dots for Bio-Application. In *Proceedings of the 20th International Congress for the International Commission for Optics: Materials and Nanostructures*; Lu, W., Young, J., Eds.; SPIE: Bellingham, WA, 2006; pp 602904–602904–6.
- (29) Zhao, H.; Chaker, M.; Wu, N.; Ma, D. *J. Mater. Chem.* **2011**, *21*, 8898.
- (30) Pietryga, J. M.; Werder, D. J.; Williams, D. J.; Casson, J. L.; Schaller, R. D.; Klimov, V. I.; Hollingsworth, J. A. *J. Am. Chem. Soc.* **2008**, *130*, 4879–4885.
- (31) Neo, M. S.; Venkatram, N.; Li, G. S.; Chin, W. S.; Ji, W. *J. Phys. Chem. C* **2010**, *114*, 18037–18044.
- (32) Ghosh Chaudhuri, R.; Paria, S. *Chem. Rev.* **2012**, *112*, 2373–2433.
- (33) Fernée, M. J.; Watt, A.; Warner, J.; Cooper, S.; Heckenberg, N.; Rubinsztein-Dunlop, H. *Nanotechnology* **2003**, *14*, 991–997.
- (34) Lifshitz, E.; Brumer, M.; Kigel, A.; Sashchiuk, A.; Bashouti, M.; Sirota, M.; Galun, E.; Burshtein, Z.; Le Quang, A. Q.; Ledoux-Rak, I.; et al. *J. Phys. Chem. B* **2006**, *110*, 25356–25365.
- (35) Ning, Z.; Tian, H.; Yuan, C.; Fu, Y.; Qin, H.; Sun, L.; Ågren, H. *Chem. Commun.* **2011**, *47*, 1536.
- (36) Vinayakan, R.; Shanmugapriya, T.; Nair, P. V.; Ramamurthy, P.; Thomas, K. G. *J. Phys. Chem. C* **2007**, *111*, 10146–10149.
- (37) Kinder, E.; Moroz, P.; Diederich, G.; Johnson, A.; Kirsanova, M.; Nemchinov, A.; O'Connor, T.; Roth, D.; Zamkov, M. *J. Am. Chem. Soc.* **2011**, *133*, 20488–20499.
- (38) Moroz, P.; Kholmicheva, N.; Mellott, B.; Liyanage, G.; Rijal, U.; Bastola, E.; Huband, K.; Khon, E.; McBride, K.; Zamkov, M. *ACS Nano* **2013**, *7*, 6964–6977.
- (39) Etgar, L.; Yanover, D.; Čapek, R. K.; Vaxenburg, R.; Xue, Z.; Liu, B.; Nazeeruddin, M. K.; Lifshitz, E.; Grätzel, M. *Adv. Funct. Mater.* **2013**, *23*, 2736–2741.
- (40) Hines, M. A.; Scholes, G. D. *Adv. Mater.* **2003**, *15*, 1844–1849.
- (41) Willis, S. M.; Cheng, C.; Assender, H. E.; Watt, A. A. R. *Nano Lett.* **2012**, *12*, 1522–1526.
- (42) Fairclough, S. M.; Tyrrell, E. J.; Graham, D. M.; Lunt, P. J. B.; Hardman, S. J. O.; Pietzsch, A.; Hennies, F.; Moghal, J.; Flavell, W. R.; Watt, A. A. R.; et al. *J. Phys. Chem. C* **2012**, *116*, 26898–26907.

- (43) Balasubramanian, S.; Ceder, G.; Kolenbrander, K. D. Three-Dimensional Epitaxy: Thermodynamic Stability Range of Coherent Germanium Nanocrystallites in Silicon Host. *MRS Proc.* **2011**, *405*.
- (44) Proffen, T.; Neder, R. B. *J. Appl. Crystallogr.* **1997**, *30*, 171–175.
- (45) Ihly, R.; Tolentino, J.; Liu, Y.; Gibbs, M.; Law, M. *ACS Nano* **2011**, *5*, 8175–8186.
- (46) Liu, T.-Y.; Li, M.; Ouyang, J.; Zaman, M. B.; Wang, R.; Wu, X.; Yeh, C.-S.; Lin, Q.; Yang, B.; Yu, K. *J. Phys. Chem. C* **2009**, *113*, 2301–2308.
- (47) Rivest, J. B.; Jain, P. K. *Chem. Soc. Rev.* **2013**, *42*, 89.
- (48) Moreels, I.; Lambert, K.; Smeets, D.; De Muynck, D.; Nollet, T.; Martins, J. C.; Vanhaecke, F.; Vantomme, A.; Delerue, C.; Allan, G.; et al. *ACS Nano* **2009**, *3*, 3023–3030.
- (49) Wyckoff, R. W. G. *Crystal Structures*; Wiley, 1971; Vol. 1.
- (50) Zhao, H.; Chaker, M.; Ma, D. *J. Mater. Chem.* **2011**, *21*, 17483.
- (51) Zhao, H.; Wang, D.; Zhang, T.; Chaker, M.; Ma, D. *Chem. Commun.* **2010**, *46*, 5301.
- (52) Neder, R. B. *Diffuse Scattering and Defect Structure Simulations: A Cook Book Using the Program DISCUS*; International Union of Crystallography Book Series; Oxford University Press: Oxford, U.K., 2008.
- (53) Zhao, N.; Osedach, T. P.; Chang, L.-Y.; Geyer, S. M.; Wanger, D.; Binda, M. T.; Arango, A. C.; Bawendi, M. G.; Bulovic, V. *ACS Nano* **2010**, *4*, 3743–3752.
- (54) Zhitomirsky, D.; Kramer, I. J.; Labelle, A. J.; Fischer, A.; Debnath, R.; Pan, J.; Bakr, O. M.; Sargent, E. H. *Nano Lett.* **2012**, *12*, 1007–1012.
- (55) Xu, F.; Ma, X.; Haughn, C. R.; Benavides, J.; Doty, M. F.; Cloutier, S. G. *ACS Nano* **2011**, *5*, 9950–9957.
- (56) Foos, E. E. *J. Phys. Chem. Lett.* **2013**, *4*, 625–632.
- (57) Kovalenko, M. V.; Scheele, M.; Talapin, D. V. *Science* **2009**, *324*, 1417–1420.
- (58) Kovalenko, M. V.; Bodnarchuk, M. I.; Zaumseil, J.; Lee, J.-S.; Talapin, D. V. *J. Am. Chem. Soc.* **2010**, *132*, 10085–10092.
- (59) Nag, A.; Kovalenko, M. V.; Lee, J.-S.; Liu, W.; Spokoyny, B.; Talapin, D. V. *J. Am. Chem. Soc.* **2011**, *133*, 10612–10620.
- (60) Fafarman, A. T.; Koh, W.; Diroll, B. T.; Kim, D. K.; Ko, D.-K.; Oh, S. J.; Ye, X.; Doan-Nguyen, V.; Crump, M. R.; Reifsnyder, D. C.; et al. *J. Am. Chem. Soc.* **2011**, *133*, 15753–15761.
- (61) Bae, W. K.; Joo, J.; Padilha, L. A.; Won, J.; Lee, D. C.; Lin, Q.; Koh, W.; Luo, H.; Klimov, V. I.; Pietryga, J. M. *J. Am. Chem. Soc.* **2012**, *134*, 20160–20168.
- (62) Ning, Z.; Ren, Y.; Hoogland, S.; Voznyy, O.; Levina, L.; Stadler, P.; Lan, X.; Zhitomirsky, D.; Sargent, E. H. *Adv. Mater.* **2012**, *24*, 6295–6299.
- (63) Zanella, M.; Maserati, L.; Pernia Leal, M.; Prato, M.; Lavieille, R.; Povia, M.; Krahne, R.; Manna, L. *Chem. Mater.* **2013**, *25*, 1423–1429.
- (64) Tang, J.; Kemp, K. W.; Hoogland, S.; Jeong, K. S.; Liu, H.; Levina, L.; Furukawa, M.; Wang, X.; Debnath, R.; Cha, D.; et al. *Nat. Mater.* **2011**, *10*, 765–771.
- (65) Wuister, S. F.; de Mello Donegá, C.; Meijerink, A. *J. Phys. Chem. B* **2004**, *108*, 17393–17397.
- (66) Barkhouse, D. A. R.; Pattantyus-Abraham, A. G.; Levina, L.; Sargent, E. H. *ACS Nano* **2008**, *2*, 2356–2362.
- (67) Greenham, N. C.; Peng, X.; Alivisatos, A. P. *Synth. Met.* **1997**, *84*, 545–546.
- (68) Cai, C. F.; Zhang, B. P.; Li, R. F.; Wu, H. Z.; Xu, T. N.; Zhang, W. H.; Zhu, J. F. *EPL Europhys. Lett.* **2012**, *99*, 37010.